ACS Combinatorial Science

Research Article

pubs.acs.org/acscombsci

Solid-State Combinatorial Screening of $ARSi_4N_7:Eu^{2+}$ (A = Sr, Ba, Ca; R = Y, La, Lu) Phosphors

Woon Bae Park, Kyung Hyun Son, Satendra Pal Singh, and Kee-Sun Sohn*

Department of Printed Electronics, World Class University Program, Sunchon National University, Sunchon, Chonnam 540-742, Korea

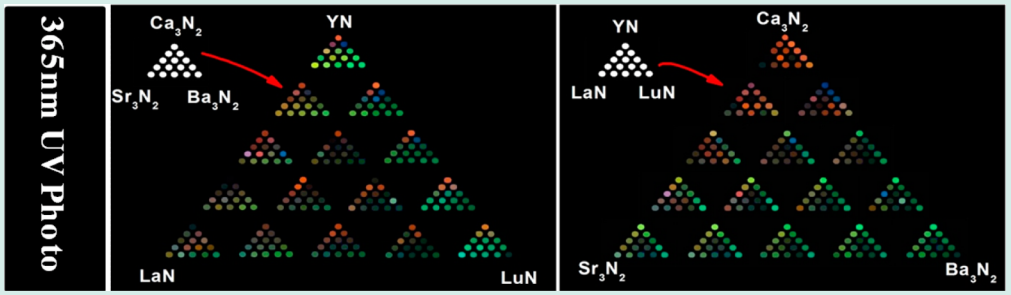

ABSTRACT: A double-ternary combinatorial chemistry (combi-chem) library was visualized in terms of structure, PL intensity, and color chromaticity for a nitride phosphor system, $ARSi_4N_7:Eu^{2+}$ (A = Sr, Ca, Ba; R = Y, La, Lu), so as to obtain a quantitative structure and property relationship (QSPR) in a systematic manner. Most of the samples constituting the double-ternary combi-chem library turned out to have $ARSi_4N_7$ structures with a $P6_3mc$ space group. However, several phases such as $Ca_2Si_5N_8$ with a Cc space group, $LaSi_3N_5$ with a $P2_12_12_1$ space group, $R_6Si_{11}N_{20}O$ with a $P31c$ space group, etc., coexisted. Aside from the green luminescence from the well-known $SrYSi_4N_7:Eu^{2+}$ and $BaYSi_4N_7:Eu^{2+}$ phosphors, their solid solutions $(Sr,Ba)Si_4N_7:Eu^{2+}$ proved to possess better PL properties. In addition, novel phosphors with an acceptable green PL intensity and color chromaticity were discovered in the $ALuSi_4N_7:Eu^{2+}$ side of the double-ternary combi-chem library. The Ca-rich side did not constitute a single-phase $ARSi_4N_7$ structure with a $P6_3mc$ space group, and therefore the red emission in the Ca-rich side proved to originate from well-known $Ca_2Si_5N_8:Eu^{2+}$ phosphors, which resided in the sample as a minor phase.

KEYWORDS: *combinatorial chemistry, phosphor, LED*

INTRODUCTION

The trend for the research of phosphors for use in light emitting diodes (LED) has dramatically moved from oxides, halides, and sulfides to either nitrides or oxynitrides, because the (oxy)nitride phosphor has proven to be superior to traditional phosphors in terms of performance and stability.[1−5] Recently developed $SrYSi_4N_7:Eu^{2+}$ and $BaYSi_4N_7:Eu^{2+}$ phosphors are reportedly a potential candidate for the green phosphors used in LEDs.[6,7] The host structure of these phosphors is an isotype of $SrYbSi_4N_7$ and $BaYbSi_4N_7$, identified as a hexagonal lattice with a $P6_3mc$ space group.[8,9] While $SrYbSi_4N_7$ and $BaYbSi_4N_7$ have never been considered candidates for a phosphor host, $SrYSi_4N_7$ and $BaYSi_4N_7$ have been of particular concern as a host material for Ce^{3+} and Eu^{2+} activation. $SrYSi_4N_7:Ce^{3+}$ and $BaYSi_4N_7:Ce^{3+}$ exhibit a blue light emission, and $SrYSi_4N_7:Eu^{2+}$ and $BaYSi_4N_7:Eu^{2+}$ exhibit green light emissions under UV excitation. The aim of the present investigation was to develop promising green light emitting phosphors based on the Eu^{2+}-activated $ARSi_4N_7:Eu^{2+}$ (A = Sr, Ca, Ba; R = Y, La, Lu) for use in LED applications.

To examine the structural and PL properties, and to discover novel compositions in the vicinity of the $SrYSi_4N_7:Eu^{2+}$ and $BaYSi_4N_7:Eu^{2+}$ compositions, which could surpass the well-known $SrYSi_4N_7:Eu^{2+}$ and $BaYSi_4N_7:Eu^{2+}$ compositions in terms of performance, it was worthwhile to track down the entire composition range involving other possible alkali earth and rare earth elements. In this regard, a combinatorial chemistry (combi-chem) technique was employed to screen a multicompositional search space based on the $ARSi_4N_7:Eu^{2+}$ stoichiometry, wherein A includes alkali earth elements such as Sr, Ca and Ba, and R represents rare earth elements such as Y, La and Lu. The conventional combi-chem strategy can conduct binary, or at best ternary, screening with a limited number of samples.[10−13] The terminology, both binary and ternary, represents only cation compositions in the present investigation. In contrast to the conventional binary and ternary combi-chem approaches, the present investigation was intended to track down a double-ternary composition system consisting of the 3 alkali earth elements and the 3 rare earth elements. By implementing the high throughput synthesis and characterization of hundreds of samples belonging to the double-ternary composition system, we completed a so-called double-ternary combi-chem library, wherein the structural and PL property was graphically represented in terms of color contour.

Received: May 29, 2012
Revised: June 19, 2012
Published: August 24, 2012

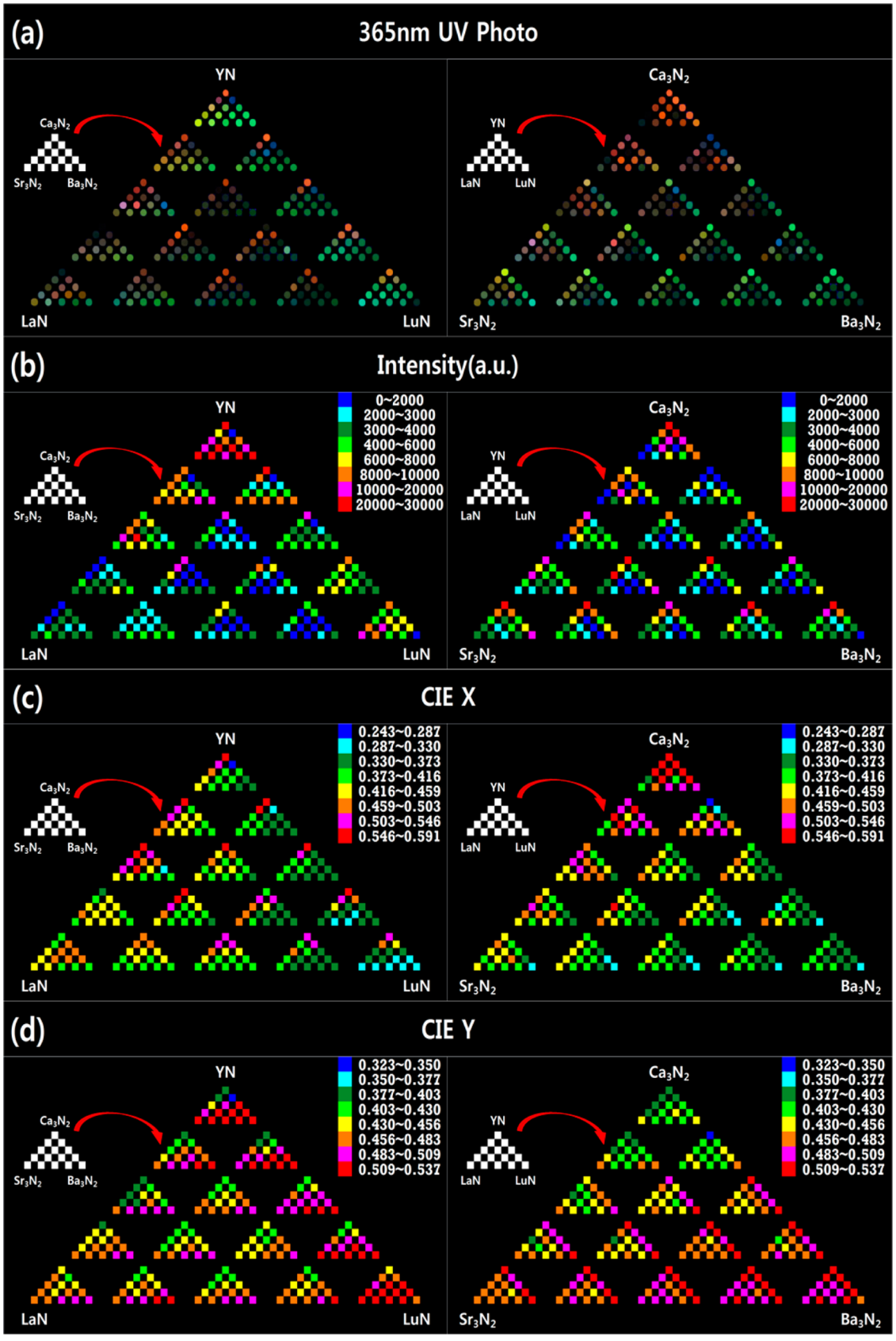

Figure 1. Double-ternary combi-chem library in terms of (a) actual photo, (b) PL intensity, and color chromaticity (c) *x* and (d) *y* values. The right and left columns refers to identical experimental results but different data representations were adopted according to the choice of the double-ternary system.

dx.doi.org/10.1021/co300057e | *ACS Comb. Sci.* 2012, 14, 537−544

A solid-state combi-chem technique is essential in the case of nitride phosphors, since some of the raw materials are air-sensitive and also extremely hygroscopic even in the air, which makes them unsuited for dissolving in certain solutions. Therefore, we have developed a powder-process-based, solid-state, high-throughput experimentation (HTE) system, which was specially designed for nitride phosphors in a dry state. More details on the solid sate HTE system are available in our previous work.[14,15] In fact, our complete combi-chem system involved heuristics optimization-assisted computational strategies along with solid-state HTE.[16] However, we did not take on the heuristics optimization-assisted computational part but employed only the HTE part in the present investigation, because we reduced significantly the composition range that we had to track down. As a result, the composition space of concern was not so large that it was not necessary to use heuristics optimization, but instead a simple HTE was sufficient. Accordingly, a total of 225 different phosphor samples evenly distributed in a so-called double-ternary composition search space were simultaneously synthesized and characterized in a high-throughput manner. As a result, a double-ternary combinatorial library was set up graphically to elucidate the quantitative composition and structure relationship (QCSR), the quantitative composition and property relationship (QCPR), and, in turn, the quantitative structure and property relationship (QSPR) for the $ARSi_4N_7:Eu^{2+}$ system.

EXPERIMENTAL PROCEDURES

The commercially available starting nitrides in the powdered state, SrN_x (Kojundo, 99%), Ca_3N_2 (Aldrich, 95%), BaN_x (Cerac, 99.7%), YN (LTS Chem., 99.5%), LaN (LTS Chem., 99.9%), LuN (Kojundo, 99%), α-Si_3N_4 (Ube, purity unreported), and EuN (Kojundo, 99.9%) were separately ground manually for several hours in a dry state prior to the mixing process. Although the exact x values were not provided by the manufacturer they should exceed 0.6. So, our weighed amount for Sr and Ba precursors based on the hypothetical Sr_3N_2 and Ba_3N_2 stoichiometry should have led to a slightly excessive amount of Sr and Ba in the final $ARSi_4N_7:Eu^{2+}$ compound. The starting materials were dispensed according to predetermined compositions in the double-ternary composition search space, and were then dry mixed in a high-throughput manner using a robotic platform (Swave, Chem-Speed Tech Co., Ltd.) in a glovebox with oxygen and a moisture content that was maintained below 2 and 1 ppm, respectively. A so-called combi-chem container, a specially designed sample container made of BN that involved 18 sample sites with a diameter of 8.5 mm and a depth of 18 mm, was devised for the high-throughput dispensing, mixing, grinding, and firing of a large number of samples. The total amount of raw materials at each sample site was around 0.3 g, which led to a sufficient amount of final phosphor powder available for use in conventional characterizations, such as with XRD and PL measurements. The exact amount of raw materials was weighed and dispensed automatically to the sample site by a powder extruder system attached to the robotic platform. The mixing and grinding was executed by vibrating the combi-chem containers with pins inserted inside the sample sites. The mixed raw materials in the combi-chem container were fired at 1600 °C for 12 h under a pressurized N_2 gas environment (5 atm) in a gas-pressurized sintering (GPS) furnace. The GPS furnace consisted of graphite heaters, a BN chamber, BN-capped thermocouples, a carbon quilt insulator, a stainless steel vessel to resist high pressure, and a water-cooling system. The stainless steel vessel and all parts were initially evacuated down to 10^{-6} Torr and heated to 1,000 °C while maintaining a high vacuum. High purity (5N) nitrogen gas, up to 10 atm, was then introduced by a mass flow controller (MFC) system. The GPS was then heated to the final temperature while the pressure inside the vessel was precisely maintained. Two combi-chem containers, 36 samples, were fired simultaneously. The Eu^{2+} content was fixed at 0.02 mol.

It should be noted that we fixed the processing conditions, which included several key parameters such as firing temperature, heating rate, firing time, gas pressure, etc. The processing conditions adopted for the construction of the combi-chem library shown in Figure 1 were selected such that a single-phase of $BaYSi_4N_7$ could be attained at a temperature that was as low as possible. In fact, we iterated many preliminary experiments focusing only on the formation of a single-phase $BaYSi_4N_7$. This meant that better quality and performance would be available for all the other phases, with the exception of $BaYSi_4N_7$, if processing conditions changed.

The fired samples were ground and subjected to X-ray diffraction (XRD), energy dispersive spectroscopy (EDS), and photoluminescence (PL). The emission spectra were monitored at 460 nm, which simulates an InGaN LED light source, with the samples being left in the combi-chem containers in a high-throughput manner using an in-house fabricated continuous wave (CW) PL system equipped with a Xenon lamp. A video, which shows the entire high-throughput dispensing and synthesis process, is available elsewhere.[14,15] XRD patterns were recorded using a Rigaku ULTIMA 4 with Cu K_α radiation in a 2θ range of 10 to 120° at a step size of 0.005 °.

Rietveld refinement was carried out using a Fullprof package[17] for 2 representative samples. In the refinement, a pseudo-Voigt function and a linear interpolation between the set background points with refinable heights were used to define the profile shape and the background, respectively. All occupancy parameters were fixed at a nominal composition, and the isotropic thermal factor was used for all atomic positions. All other parameters, such as scale factor, zero correction, background, half-width parameters, the mixing parameters, lattice parameters, positional coordinates, and thermal parameters, were varied in the course of refinement.

RESULTS AND DISCUSSION

Both $SrYSi_4N_7:Eu^{2+}$ and $BaYSi_4N_7:Eu^{2+}$ phosphors are well-known to give a promising green emission at soft UV excitations.[6,7] Once a promising phosphor was developed, it was customary to substitute its element for several other elements from the periodic table, particularly from the same group, and thereby to produce a solid solution to a certain composition limit with the original structure maintained in an attempt to get better PL properties. In this context, there have been many successful developments of solid solution-type phosphors such as $(Sr,Ba)_2SiO_4:Eu^{2+}$ and $(Sr,Ca)AlSiN_3:Eu^{2+}$, which have been commercially available. Although it is easy to make a binary solid-solution series in a limited composition range, the full screening of a ternary solid solution would not be a simple job if a conventional one-by-one strategy was employed. Furthermore, when the task to be accomplished exceeded the ternary composition system, it would be extremely difficult to screen the entire composition range. In this case, we were faced with a so-called double-ternary

dx.doi.org/10.1021/co300057e | ACS Comb. Sci. 2012, 14, 537−544

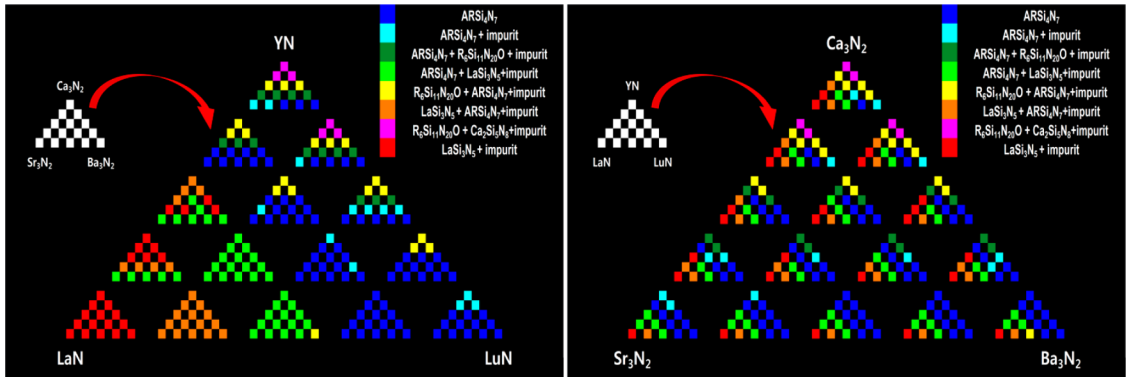

Figure 2. Double-ternary combi-chem library in terms of the constituent phase. The third minor phase was not given here, specifically, but was represented as just an impurity. However, most of them included the $Ca_2Si_5N_8$ phase.

composition system, consisting of the ternary alkali earth elements (Ca, Sr, Ba), as well as the ternary rare earth elements (Y, La, Lu). Namely, these alkali earth and rare earth elements constituted the A and R sites in the $ARSi_4N_7:Eu^{2+}$ structure, respectively. It would not be sufficient to fully screen the double-ternary composition system using a simple one-by-one strategy. In this regard, a combi-chem approach is inevitable and simultaneously an appropriate HTE for the phosphor synthesis and characterization should be employed. In addition, by considering the fact that most commercially available phosphors are prepared using a solid-state, powder-based process, the combi-chem approach should be based on the solid-state powder synthesis. The conventional HTE that is based on inkjet and thin-film technologies would not be suitable for the combi-chem of phosphors.[16]

Figure 1a, b, c, and d shows the double-ternary combi-chem library in terms of actual photo, PL intensity, and color chromaticity *x* and *y* values. The double-ternary combi-chem library is composed of a large ternary diagram with 15 small ternary diagrams on the inside. The apex component of the large ternary library located on the right side of Figure 1 are alkali earth elements (Sr, Ba, Ca) while those for the small ternary library inside the larger one are rare earth elements (Y, La, Lu), and vice versa for the left-side library. By exhibiting the same combi-chem results in 2 different ways as presented on the right and left sides of Figure 1, we were able to comprehend the relationship between the composition and properties in a more systematic way. The scale bar located in the upper right side of each diagram shows the numeric values of PL intensity, and color chromaticity *x* and *y*, so that those values can be recognized in terms of color contour in the double-ternary combi-chem library.

Figure 1a represents actual photos taken at 360 nm UV lamp excitations. Although the quantitative results were separately summarized in Figure 1b, c, and d, the actual photos in Figure 1a provided a more vivid representation of the combi-chem results. A variety of emission colors were available in this double-ternary combi-chem library, which was due to the unshielded nature of the 5d → 4f transition of divalent europium activators. This meant that the different composition of each sample in the combi-chem library gave rise to various local environments around the Eu^{2+} activator, which brought about their corresponding neuplauxetic effects, crystal field strengths, and Stokes shifts.[18] This eventually affected the emission colors. It is evident that the emission color observed in Figure 1a spanned from blue, green, and yellow to red colors.

Although we fixed the composition of alkali earth, rare earth, silicon nitride, and europium activators as $ARSi_4N_7:Eu^{2+}_{0.02}$, the final structure of samples in the double-ternary combi-chem library was not always the $ARSi_4N_7:Eu^{2+}_{0.02}$ structure with a $P6_3mc$ space group. Some areas in the double-ternary combi-chem library turned out to be comprised of 2 or more impurity phases along with the $ARSi_4N_7:Eu^{2+}_{0.02}$ phase. Moreover, the $ARSi_4N_7:Eu^{2+}_{0.02}$ phase did not appear at all in some extreme cases; instead, only impurity phases were detected. In this case, some of the constituent phases were luminescent and some were not. Figure 2 shows the double-ternary combi-chem library in terms of the constituent phase, which was constructed using the XRD measurement results for all of the phosphor samples. Major constituent compounds detected in the double-ternary combi-chem library were $ARSi_4N_7:Eu^{2+}$ (A = Sr, Ba, R = Y, Lu) phosphors with a $P6_3mc$ space group.[6,7] In addition to these main phases, several minor constituent compounds such as $Ca_2Si_5N_8$ with a *Cc* space group,[19] $LaSi_3N_5$ with a $P2_12_12_1$ space group,[20] and $R_6Si_{11}N_{20}O$ with a *P*31c space group were also clearly observed in many samples.[21] Several unidentified minor phases and starting materials were also detected even though their amount was negligible. The double-ternary combi-chem library was constructed in terms of the constituent phase, as shown in Figure 2. It should be noted that this phase library construction was based only on 3, or less, major phases detected in the XRD pattern of each sample.

The phase identification of each sample in the double-ternary combi-chem library was essential since we had to know which constituent compound actually took a part of luminescence and which did not. For instance, we detected a certain degree of red-colored light emission in some areas of the double-ternary combi-chem library, as can be clearly seen in Figure 1a. Figure 2 shows that most of the samples exhibiting red emissions included $R_6Si_{11}N_{20}O$ with a *P*31c space group as a main phase. This might have led to the wrong assumption that the $R_6Si_{11}N_{20}O$ phase plays an appropriate role in hosting the Eu^{2+} activator and thereby giving rise to red emissions. However, it is certain that the $R_6Si_{11}N_{20}O:Eu^{2+}$ was not responsible for the observed red emissions. Instead, well-known $Ca_2Si_5N_8:Eu^{2+}$ phosphors or $Ca_2Si_5N_8:Eu^{2+}$-based solid-solution phosphors proved to be the cause of the red emissions. Because it was possible to detect the red emissions for all samples that involved $Ca_2Si_5N_8$ or $Ca_2Si_5N_8$-based solid solutions as either a second or third minor constituent phase. To verify this, we succeeded in synthesizing a nearly pure $R_6Si_{11}N_{20}O:Eu^{2+}$ phase and eventually confirmed that there was no red emission from

dx.doi.org/10.1021/co300057e | *ACS Comb. Sci.* 2012, 14, 537−544

the single phase of $R_6Si_{11}N_{20}O:Eu^{2+}$. Accordingly, it was proved that the $R_6Si_{11}N_{20}O$ phase was not a good host for the Eu^{2+} activator.

Referring to the phase identification results shown in Figure 2, we realized that although the processing composition was fixed to the $ARSi_4N_7:Eu^{2+}$ stoichiometry in the synthesis process, the final samples did not crystallize into single-phase $ARSi_4N_7:Eu^{2+}$ but instead ended up with a lot of unexpected phases. It should be noted that it is rare to see a case where the processing composition coincides exactly with the actual stoichiometry. The processing composition generally has nothing to do with the actual stoichiometry of final samples in most inorganic compound syntheses. It is evident that the processing composition had little influence on the final stoichiometry, but that the synthesis conditions had more of an effect in achieving the single-phase compound that we had targeted. One should notice that there is an appropriate processing composition in order to achieve a single-phase phosphor, and this processing composition often differs significantly from the desired stoichiometry.

As expected according to the literature,[6,7] a promising green emission was observed around the $SrYSi_4N_7:Eu^{2+}$ and $BaYSi_4N_7:Eu^{2+}$ corner in the double-ternary combi-chem library. It was also possible to achieve a promising green emission in a series of binary solid solutions between $SrYSi_4N_7:Eu^{2+}$ and $BaYSi_4N_7:Eu^{2+}$ phosphors. Figure 3a and b show the XRD patterns and emission spectra for a series of binary solid solutions between $SrYSi_4N_7:Eu^{2+}$ and $BaYSi_4N_7:Eu^{2+}$ phosphors. Because the structure of $SrYSi_4N_7$ and $BaYSi_4N_7$ is identical, the XRD patterns for $(Sr,Ba)YSi_4N_7:Eu^{2+}$ phosphors were all similar, which means that homogeneous solid solutions were obtained between $SrYSi_4N_7:Eu^{2+}$ and $BaYSi_4N_7:Eu^{2+}$ phosphors. The calculated XRD patterns based on the refined structure of $SrYSi_4N_7$ and $BaYSi_4N_7$ phases[6,7] were also identical, as shown in Figure 3a. Although a slight amount of the impurity phase was detected in the $SrYSi_4N_7:Eu^{2+}$ side, only a well-defined, single-phase $(Sr,Ba)YSi_4N_7:Eu^{2+}$, solid-solution phase appeared as the amount of Ba increased. It is evident that $(Ba_{0.25}Sr_{0.75})YSi_4N_7:Eu^{2+}$ showed the highest PL intensity and more importantly the emission band location of binary $(Sr,Ba)YSi_4N_7:Eu^{2+}$ solid-solution phosphors blue-shifted as the amount of Ba increased. The peak location shifted from 560 to 530 nm as the binary composition moved from $SrYSi_4N_7:Eu^{2+}$ to $BaYSi_4N_7:Eu^{2+}$. The color chromaticity coordinates shifted along a certain line in the chromaticity diagram, as shown in Figure 4. This sort of shift has been observed in many binary solid-solution phosphors such as $(Sr,Ba)_2SiO_4:Eu^{2+}$, $(Sr,Ba)_2Si_5N_8:Eu^{2+}$, $(Sr,Ba)Si_2N_2O_2:Eu^{2+}$, and $(Sr,Ca)AlSiN_3:Eu^{2+}$.[1−5] This behavior should be due to the lattice strain caused by the size difference between alkali earth elements. More precisely, the local structure variation with respect to the random distribution of different alkali earth elements at the same crystallographic site in the structure should provide the Eu^{2+} activator with various local environments and eventually affect the nephelauxetic effect, the crystal field strength, and the Stokes shift.[18] Consequently, the PL intensity could be improved and the emission color could be fine-tuned by constituting a binary solid solution between the $SrYSi_4N_7:Eu^{2+}$ and $BaYSi_4N_7:Eu^{2+}$ phosphors. In this respect, the binary $(Sr,Ba)YSi_4N_7:Eu^{2+}$ solid-solution phosphors deserved to be recommended instead of the conventional $SrYSi_4N_7:Eu^{2+}$ and $BaYSi_4N_7:Eu^{2+}$ phosphors.

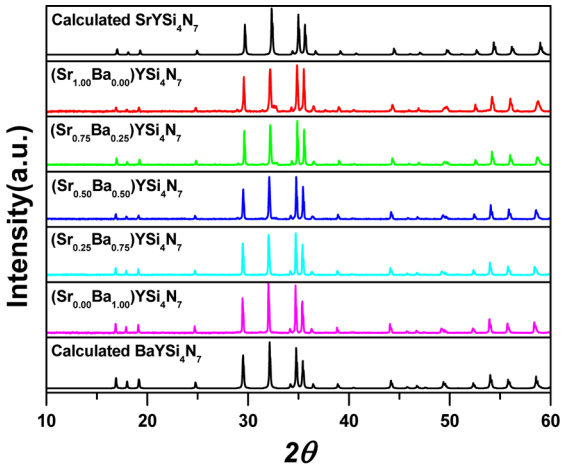

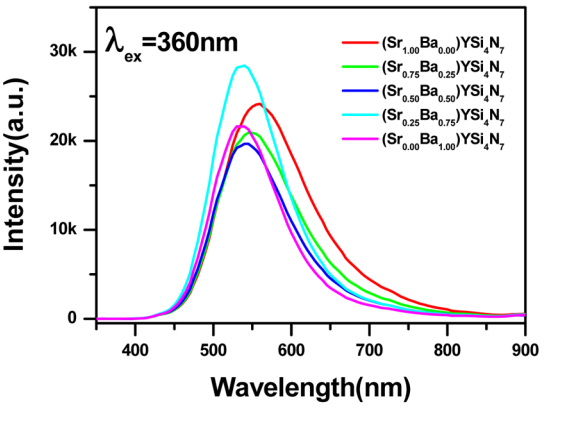

Figure 3. (a) XRD patterns and (b) emission spectra for a series of binary solid solutions between $SrYSi_4N_7:Eu^{2+}$ and $BaYSi_4N_7:Eu^{2+}$ phosphors.

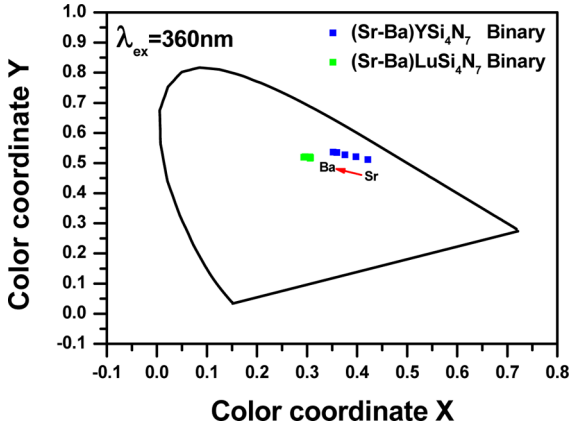

Figure 4. Color chromaticity coordinates both for $(Sr,Ba)YSi_4N_7:Eu^{2+}$ and $(Sr,Ba)LuSi_4N_7:Eu^{2+}$ solid-solution phosphors, which were marked as blue and green dots, respectively.

Although the advantage of binary $(Sr,Ba)YSi_4N_7:Eu^{2+}$ solid-solution phosphors was an interesting new result, what interested us most was neither the well-known $SrYSi_4N_7:Eu^{2+}$ and $BaYSi_4N_7:Eu^{2+}$ phosphors nor their solid solutions, but instead potential novel phosphors was our major concern in the present combi-chem approach. Novel phosphors were dis-

dx.doi.org/10.1021/co300057e | ACS Comb. Sci. 2012, 14, 537−544

covered particularly in the $SrLuSi_4N_7:Eu^{2+}$ and $BaLuSi_4N_7:Eu^{2+}$ corner of the double-ternary combi-chem library. As shown in Figure 1a and b, the PL intensity for $SrLuSi_4N_7:Eu^{2+}$ and binary $(Sr,Ba)LuSi_4N_7:Eu^{2+}$ solid-solution phosphors seemed acceptable even though the relative intensity was inferior to that of the binary $(Sr,Ba)YSi_4N_7:Eu^{2+}$ solid-solution phosphors. The PL intensity of $BaLuSi_4N_7:Eu^{2+}$ was not comparable to $SrLuSi_4N_7:Eu^{2+}$. The $SrLuSi_4N_7:Eu^{2+}$, $BaLuSi_4N_7:Eu^{2+}$, and $(Sr,Ba)LuSi_4N_7$ phosphors are novel since they have never been synthesized, and, therefore, have never been considered as host materials for Eu^{2+} activators. Figure 5a and b show the

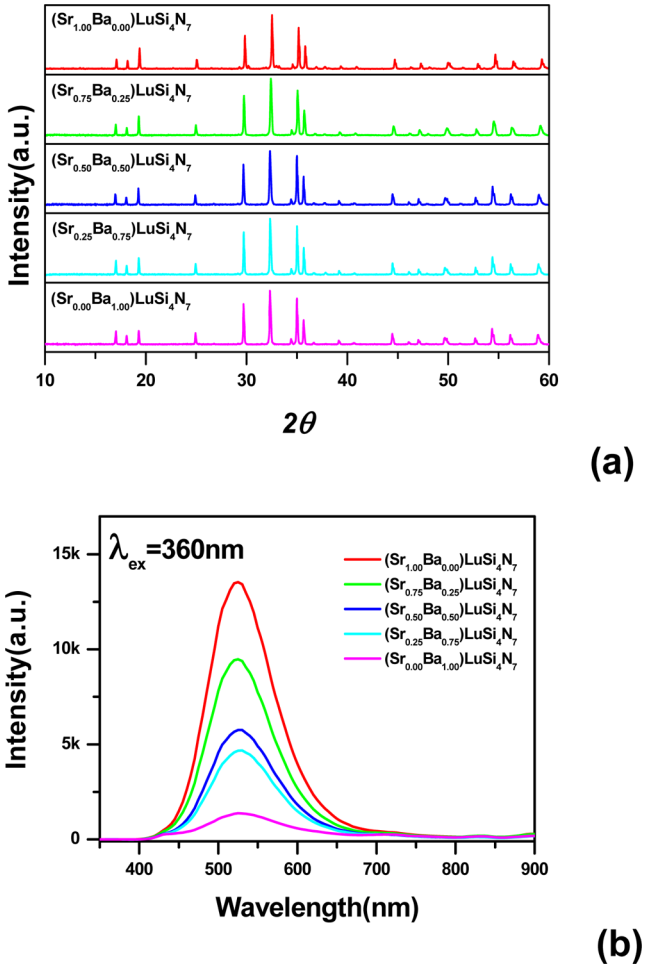

Figure 5. (a) XRD patterns and (b) emission spectra for a series of binary solid solutions between $SrLuSi_4N_7:Eu^{2+}$ and $BaLuSi_4N_7:Eu^{2+}$ phosphors.

XRD patterns and emission spectra for a series of binary solid solutions between $SrLuSi_4N_7:Eu^{2+}$ and $BaLuSi_4N_7:Eu^{2+}$ phosphors. Although a slight amount of the impurity phase was detected, well-defined single phases were clearly obtained in most of the $(Sr,Ba)LuSi_4N_7:Eu^{2+}$ phosphors. The PL results showed that the emission peak position was blue-shifted significantly in comparison with $(Sr,Ba)YSi_4N_7:Eu^{2+}$ phosphors. Unlike the $SrYSi_4N_7:Eu^{2+}$ and $BaYSi_4N_7:Eu^{2+}$ binary system, wherein both sides proved to be good phosphors, only the $SrLuSi_4N_7:Eu^{2+}$ phosphor turned out to be a good phosphor, but $BaLuSi_4N_7:Eu^{2+}$ did not constitute a good phosphor. Also, the $(Sr,Ba)LuSi_4N_7:Eu^{2+}$ solid-solution phosphors had no merit, since the greater amount of Ba doping in the $SrLuSi_4N_7:Eu^{2+}$ phosphor induced a lower PL intensity. It is also interesting that there was no emission band shift with respect to the Ba doping. The peak position was fixed at 525 nm all the time, which led to the invariant color chromaticity coordinate values, as shown in Figure 4.

To give a more reliable structural analysis to both $SrLuSi_4N_7:Eu^{2+}$ and $BaLuSi_4N_7:Eu^{2+}$, we carried out Rietveld analysis on the powder X-ray diffraction data. Figure 6a and b

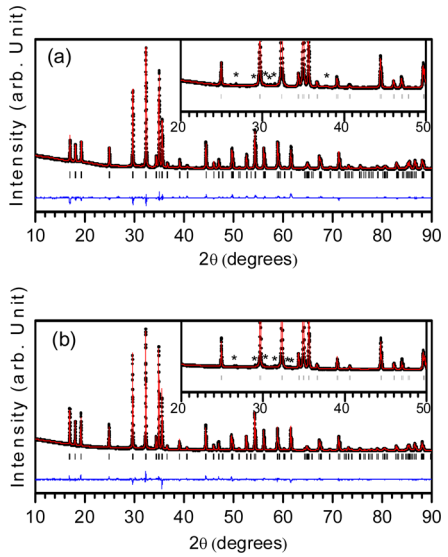

Figure 6. Observed (dots), calculated (red line) and difference (blue line) profiles obtained after full-pattern Rietveld refinement using a hexagonal structure in the $P6_3mc$ space group for (a) $BaLuSi_4N_7$ and (b) $SrLuSi_4N_7$. The unidentified impurity phases are marked with an asterisk (*) in the inset to the figures. The tick marks above the difference profile denotes the position of Bragg reflections.

shows the fit between the observed and calculated data obtained after the Rietveld refinement. The list of refined structural parameters along with the occupancy and Wyckoff sites are shown in Table 1. According to current related literature,[6−9] alkali earth elements such as Sr and Ba and rare earth elements such as Y and Yb occupy different crystallographic sites even though they belong to the same Wyckoff site (*2b*). We tried to refine the structure by assigning similar atomic positions to Sr/Ba and Lu as per those of $SrYSi_4N_7:Eu^{2+}$ and $BaYSi_4N_7:Eu^{2+}$, as reported in the literature,[6,7] but this gave an unusually large variation in the thermal parameters, which is an indication of the wrong site assignment. An interchange of the Sr/Ba and Lu sites also resulted in a similar variation in the thermal parameters with a comparable fit quality and χ^2 values. Therefore, Rietveld refinement was carried out by sharing the 2b Wyckoff site in equal proportion (50:50) by both the alkali earth and the Lu ion, which resulted in a very good agreement between the observed and calculated patterns with acceptable values of thermal parameters and the agreement factors. Although a slight amount of the impurity phase was detected for both $SrLuSi_4N_7$ and $BaLuSi_4N_7$, this was not taken into account during the refinement process and resulted in slightly higher values for the agreement factors, such as R_p, R_{wp}, R_{exp}, and χ^2. We were able to index a few of the impurity peaks with SrO in $SrLuSi_4N_7$, but we could not identify the impurity phases present in $BaLuSi_4N_7$.

Figure 7 shows the excitation spectra for $SrYSi_4N_7:Eu^{2+}$, $BaYSi_4N_7:Eu^{2+}$, $SrLuSi_4N_7:Eu^{2+}$, and $BaLuSi_4N_7:Eu^{2+}$. The

dx.doi.org/10.1021/co300057e | ACS Comb. Sci. 2012, 14, 537−544

Table 1. Refined Structural Parameters of $BaLuSi_4N_7$ and $SrLuSi_4N_7$

			$BaLuSi_4N_7$[a]			
atom	Wyckoff site	*x*/*a*	*y*/*b*	*z*/*c*	*B* (Å^2)	occ.
Lu	2*b*	0.3333	0.6667	0.4507(7)	0.10(2)	0.5
Ba	2*b*	0.3333	0.6667	0.4507(7)	0.10(2)	0.5
Lu	2*b*	0.3333	0.6667	0.07627)	0.21(4)	0.5
Ba	2*b*	0.3333	0.6667	0.0762(7)	0.21(4)	0.5
Si1	2*a*	0.0000	0.0000	0.5296(10)	0.31(1)	1.0
Si2	6*c*	0.8324(5)	0.6643(5)	0.2650(11)	0.38(4)	1.0
N1	6*c*	0.5280(5)	0.4720(5)	0.3115(8)	0.29(5)	1.0
N2	6*c*	0.1345(12)	0.2691(11)	0.5758(9)	0.43(3)	1.0
N3	2*a*	0.0000	0.0000	0.3486(13)	0.38(4)	1.0
			$SrLuSi_4N_7$[b]			
atom	Wyckoff site	*x*/*a*	*y*/*b*	*z*/*c*	*B* (Å^2)	occ.
Lu	2*b*	0.3333	0.6667	0.4781(7)	0.10(2)	0.5
Sr	2*b*	0.3333	0.6667	0.4781(7)	0.10(2)	0.5
Lu	2*b*	0.3333	0.6667	0.1044(7)	0.29(2)	0.5
Sr	2*b*	0.3333	0.6667	0.1044(7)	0.29(2)	0.5
Si1	2*a*	0.0000	0.0000	0.5605(10)	0.46(3)	1.0
Si2	6*c*	0.8255(4)	0.6509(4)	0.2751(6)	0.48(2)	1.0
N1	6*c*	0.4987(6)	0.5013(4)	0.3654(8)	0.30(4)	1.0
N2	6*c*	0.1506(13)	0.3012(13)	0.5936(8)	0.69(3)	1.0
N3	2*a*	0.0000	0.0000	0.3506(14)	0.86 (4)	1.0

[a] $a = b = 6.02113(2)$, $c = 9.80105(7)$, $\alpha = \beta = 90°$, $\gamma = 120°$, space group $P6_3mc$, $R_p = 14.9$, $R_{wp} = 13.7$, $R_{exp} = 8.56$, $\chi^2 = 2.55$ $BaLuSi_4N_7$. [b] $a = b = 6.02185(2)$, $c = 9.81219$ (7), $\alpha = \beta = 90°$, $\gamma = 120°$, space group $P6_3mc$, $R_p = 13.8$, $R_{wp} = 12.7$, $R_{exp} = 8.35$, $\chi^2 = 2.31$ $SrLuSi_4N_7$

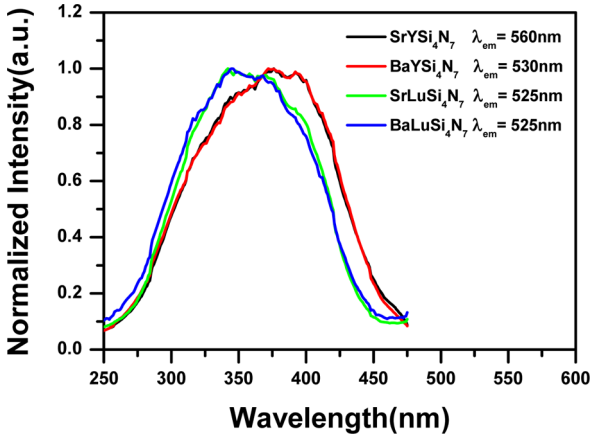

Figure 7. Excitation spectra for $SrYSi_4N_7:Eu^{2+}$, $BaYSi_4N_7:Eu^{2+}$, $SrLuSi_4N_7:Eu^{2+}$, and $BaLuSi_4N_7:Eu^{2+}$. The emission detection wavelength was fixed at the peak position of each phosphor.

excitation spectra could be divided into 2 categories conspicuously depending on whether the rare earth site was occupied by Y or Lu. As was the case for the emission spectrum peak positions, the peak positions of $SrLuSi_4N_7:Eu^{2+}$ and $BaLuSi_4N_7:Eu^{2+}$ were located in the shorter wavelength side by comparison with those of $SrYSi_4N_7:Eu^{2+}$ and $BaYSi_4N_7:Eu^{2+}$. According to the excitation spectra in Figure 7, these phosphors are suitable for UV chip-based-LED applications. It is very interesting that the excitation spectra of $SrYSi_4N_7:Eu^{2+}$ and $BaYSi_4N_7:Eu^{2+}$ were in very good agreement. Also, (Sr,Ba)-$YSi_4N_7:Eu^{2+}$ solid-solution phosphors exhibited an identical excitation spectrum with no peak shift. This behavior is incompatible with the result where the emission peak shift was prominent between $SrYSi_4N_7:Eu^{2+}$ and $BaYSi_4N_7:Eu^{2+}$. A reasonable explanation for this incompatibility is that such a dramatic shift in the emission peak location was mostly because of a different Stokes shift. This implies that the energy baricenter and the crystal field splitting had little influence on the emission peak shift.

CONCLUSION

A solid-state combi-chem approach was employed to screen a nitride-based phosphor system: the $ARSi_4N_7:Eu^{2+}$ system (A = Sr, Ca, Ba; R = Y, La, Lu). As a result, we could construct a comprehensive combi-chem library, a so-called double-ternary combi-chem library, elucidating the quantitative structure and property relationships for the $ARSi_4N_7:Eu^{2+}$ system. Even though well-known $SrYSi_4N_7:Eu^{2+}$ and $BaYSi_4N_7:Eu^{2+}$ phosphors were again confirmed as showing promise in the double-ternary combi-chem library, we also discovered novel phosphors that showed acceptable PL properties. This novel discovery included $SrLuSi_4N_7:Eu^{2+}$ and $(Sr,Ba)YSi_4N_7:Eu^{2+}$ solid-solution phosphors, which could be good candidates for LED applications. The Rietveld refinement for $SrLuSi_4N_7:Eu^{2+}$ revealed that the atomic arrangement differed slightly from the well-known $SrYSi_4N_7:Eu^{2+}$ and $BaYSi_4N_7:Eu^{2+}$ phosphors, even though the structure was identical. The maximum PL intensity was detected in the $SrYSi_4N_7:Eu^{2+}$ and $BaYSi_4N_7:Eu^{2+}$ binary solid-solution phosphors, and better color chromaticity was found for a blue-shifted $SrLuSi_4N_7:Eu^{2+}$ phosphor.

AUTHOR INFORMATION

Corresponding Author

*E-mail: kssohn@sunchon.ac.kr.

Notes

The authors declare no competing financial interest.

ACKNOWLEDGMENTS

This work was supported by the IT R&D program of MKE/IITA (2009-F-020-01) and partly supported by the WCU

(World Class University) program funded by the Ministry of Education, Science and Technology.

REFERENCES

(1) Hirosaki, N.; Xie, R.-J.; Kimoto, K.; Sekiguchi, T.; Yamamoto, Y.; Suehiro, T.; Mitomo, M. Characterization and properties of green-emitting β-SiAlON:Eu^{2+} powder phosphors for white light-emitting diodes. *Appl. Phys. Lett.* **2005**, *86*, 211905.

(2) Uheda, K.; Hirosaki, N.; Yamamoto, Y.; Naito, A.; Nakajima, T.; Yamamoto, H. Luminescence properties of a red phosphor, $CaAlSiN_3$:Eu^{2+}, for white light-emitting diodes. *Electrochem. Sol. Stat. Lett.* **2006**, *9*, H22−H25.

(3) Xie, R.-J.; Hirosaki, N.; Suehiro, T.; Xu, F.-F.; Mitomo, M. A simple, efficient synthetic route to $Sr_2Si_5N_8$:Eu^{2+}-based red phosphors for white light-emitting diodes. *Chem. Mater.* **2006**, *18*, 5578−5583.

(4) Li, Y. Q.; Delsing, A. C. A.; de With, G.; Hintzen, H. T. Luminescence properties of Eu^{2+}-activated alkaline-earth silicon-oxynitride $MSi_2O_{2-\delta}N_{2+2/3\delta}$ (M = Ca, Sr, Ba): A promising class of novel LED conversion phosphors. *Chem. Mater.* **2005**, *17*, 3242−3248.

(5) Hecht, C.; Stadler, F.; Schmidt, P. J.; Schmedt auf der Günne, J.; Baumann, V.; Schnick, W. $SrAlSi_4N_7$:Eu^{2+}—A nitridoalumosilicate phosphor for warm white light (pc)LEDs with edge-sharing tetrahedra. *Chem. Mater.* **2009**, *21*, 1595−1601.

(6) Li, Y. Q. Structure and luminescence properties of novel rare-earth doped silicon nitride based materials. Ph.D. Thesis, Eindhoven University of Technology, Eindhoven, The Netherlands, 2005.

(7) Li, Y. Q.; Fang, C. M.; de With, G.; Hintzen, H. T. Preparation, structure and photoluminescence properties of Eu^{2+} and Ce^{3+}-doped $SrYSi_4N_7$. *J. Solid State Chem.* **2004**, *177*, 4687−4694.

(8) Huppertz, H.; Schnick, W. Synthesis, crystal structure, and properties of the nitridosilicates $SrYbSi_4N_7$ and $BaYbSi_4N_7$. *Z. Anorg. Allg. Chem.* **1997**, *623*, 212−217.

(9) Fang, C. M.; Li, Y. Q.; Hintzen, H. T.; de With, G. Crystal and electronic of the novel nitrides MSi_4N_7(M = Sr, Ba) with peculiar NSi_4 coordination. *J. Mater. Chem.* **2003**, *13*, 1480−1483.

(10) Chan, T.-S.; Liu, Y.-M.; Liu, R.-S. Combinatorial search for green and blue phosphors of high thermal stabilities under UV excitation based on the $K(Sr_{1-x-y})PO_4$:$Tb^{3+}{}_xEu^{2+}{}_y$ system. *J. Comb. Chem.* **2008**, *10*, 847−850.

(11) Chen, L.; Fu, Y.; Zhang, G.; Bao, J.; Gao, C. Optimization of Pr^{3+}, Tb^{3+}, and Sm^{3+} Co-Dored $(Y_{0.65}Gd_{0.35})BO_3$:$Eu_{0.05}{}^{3+}$ VUV phosphors through combinatorial approach. *J. Comb. Chem.* **2008**, *10*, 401−404.

(12) Chen, L.; Bao, J.; Gao, C. Combinatorial synthesis of insoluble oxide library from ultrafine/nano particle suspension using a drop-on-demand inkjet delivery system. *J. Comb. Chem.* **2004**, *6*, 699−702.

(13) Chan, T.-S.; Kang, C.-C.; Liu, R.-S.; Chen, L.; Liu, X.-N.; Ding, J.-J.; Bao, J.; Gao, C. Combinatorial study of the optimization of Y_2O_3:Bi,Eu red phosphors. *J. Comb. Chem.* **2007**, *9*, 343−346.

(14) Lee, B.; Lee, S.; Jeong, H. G.; Sohn, K.-S. Solid-state combinatorial screening of $(Sr,Ca,Ba,Mg)_2Si_5N_8$:Eu^{2+} phosphors. *ACS Comb. Sci.* **2011**, *13*, 154−158.

(15) Park, W. B.; Singh, S. P.; Pyo, M.; Sohn, K.-S. $Y_{6+x/3}Si_{11-y}Al_yN_{20+x-y}O_{1-x+y}$:$Re^{3+}$ (Re = Ce^{3+}, Tb^{3+}, Sm^{3+}) phosphors identified by solid-state combinatorial chemistry. *J. Mater. Chem.* **2011**, *21*, 5780−5785.

(16) Park, W. B.; Shin, N.; Hong, K.-P.; Pyo, M.; Sohn, K.-S. A new paradigm for materials discovery: Heuristics-assisted combinatorial chemistry involving parameterization of material novelty. *Adv. Funct. Mater.* **2012**, *22*, 2258−2266.

(17) Rodriguez-Carvajal, J. *FULLPROF*; Laboratory Leon Brillouin CEA-CNRSCEA/Saclay: Gif sur Yvette Cedex, France, 2010.

(18) Xie, R.-J.; Li, Q. Y.; Hirosaki, N.; Yamamoto, H. *Nitride Phosphors and Solid-State Lighting*; CRC Press: New York, 2011.

(19) Schlieper, T.; Schnick, W.; Nitrido-Silicate., I. Hochtemperatur-synthese und kristallstruktur von Ca2Si5N8. *Z. Anorg. Allg. Chem.* **1995**, *621*, 1037.

(20) Inoue, Z.; Mitomo, M.; Ii, N. A crystallographic study of a new compound of lanthanum silicon nitride, $LaSi_3N_5$. *J. Mater. Sci.* **1980**, *15*, 2915−2920.

(21) Köllisch, K.; Höppe, H. A.; Huppertz, H.; Orth, M.; Schnick, W. New representatives of the $Er_6[Si_{11}N_{20}]O$ structure type. High-temperature synthesis and single-crystal structure refinement of $Ln_{(6+x/3)}[Si_{(11-y)}Al_yN_{(20+x-y)}]O_{(1-x+y)}$ with Ln = Nd, Er, Yb, Dy and $0 \le x \le 3$, $0 \le y \le 3$. *Z. Anorg. Allg. Chem.* **2001**, *627*, 1371−1376.